PERGAMON

Atmospheric Environment 36 (2002) 4541–4554

ATMOSPHERIC ENVIRONMENT

www.elsevier.com/locate/atmosenv

Origins of fine aerosol mass in the Baltimore–Washington corridor: implications from observation, factor analysis, and ensemble air parcel back trajectories

L.-W. Antony Chen[a], Bruce G. Doddridge[a,b,*], Russell R. Dickerson[a,b], Judith C. Chow[c], Ronald C. Henry[d]

[a] *Chemical Physics Program, University of Maryland, College Park, MD 20742, USA*
[b] *Department of Meteorology, University of Maryland, College Park, MD 20742, USA*
[c] *Atmospheric Science Division, Desert Research Institute, 2215 Raggio Parkway, Reno, NV 89512, USA*
[d] *Department of Civil and Environmental Engineering, University of Southern California, Los Angeles, CA 90089, USA*

Received 15 March 2002; accepted 28 May 2002

Abstract

Chemically speciated fine particulate matter ($PM_{2.5}$) and trace gases (including NH_3, HNO_3, CO, SO_2, NO_y) have been sampled at Fort Meade (FME: 39.10°N, 76.74°W; elevation 46 m MSL), Maryland, since July 1999. FME is suburban, located in the middle of the Baltimore–Washington corridor, and generally downwind of the highly industrialized Midwest. The $PM_{2.5}$ at FME is expected to be of both local and regional sources. Measurements over a 2-year period include eight seasonally representative months. The $PM_{2.5}$ shows an annual mean of $13\,\mu g\,m^{-3}$ and primarily consists of sulfate, nitrate, ammonium, and carbonaceous material. Day-to-day and seasonal variations in the $PM_{2.5}$ chemical composition reflect changes of contribution from various sources. UNMIX, an innovative receptor model, is used to retrieve potential sources of the $PM_{2.5}$. A six-factor model, including regional sulfate, local sulfate, wood smoke, copper/iron processing industry, mobile, and secondary nitrate, is constructed and compared with reported source emission profiles. The six factors are studied further using an ensemble back trajectory method to identify possible source locations. Sources of local sulfate, mobile, and secondary nitrate are more localized around the receptor than those of other factors. Regional sulfate and wood smoke are more regional and associated with westerly and southerly transport, respectively. This study suggests that the local contribution to $PM_{2.5}$ mass can vary from $<30\%$ in summer to $>60\%$ in winter.

Keywords: Aerosol chemical composition; Multivariance receptor model; $PM_{2.5}$ source apportionment; Air pollution meteorology

1. Introduction

In the last decade, there has been a growing concern about the health and environmental effects of urban fine aerosols. Epidemiological studies have demonstrated statistical associations between short-term increase in ambient aerosol concentration and daily mortality/morbidity (Dockery et al., 1993). Fine aerosols are essential to the formation of smog or haze that causes light extinction and reduces visibility. In 1997, the United States Environmental Protection Agency (US-EPA) classified fine particulate matter as a criteria air pollutant and added new annual ($15\,\mu g\,m^{-3}$) and 24-h ($65\,\mu g\,m^{-3}$) standards of ambient $PM_{2.5}$ (particles with aerodynamic mean diameters at or below 2.5 μm) mass

*Corresponding author. Department of Meteorology, University of Maryland, College Park, MD 20742, USA. Tel.: +1-301-405-7628; fax: +1-301-314-9482.
E-mail address: bruce@atmos.umd.edu (B.G. Doddridge).

1352-2310/02/$ - see front matter
PII: S1352-2310(02)00399-0

concentration to the National Ambient Air Quality Standard (NAAQS). The heavily populated US eastern seaboard is among the regions where haze and smog are frequently observed (Malm, 1992). Designing control strategies to bring the $PM_{2.5}$ level into compliance with the NAAQS will require knowledge of the aerosol chemical composition and source contribution. Field studies conducted in this region suggest that ammonium sulfate and carbonaceous material dominate the $PM_{2.5}$ mass (Malm et al., 1994). Sulfate (SO_4^{2-}) originates mostly from the oxidation of sulfur dioxide (SO_2), and the major sources of SO_2 in North America include coal-burning utility plants. Carbonaceous aerosols, consisting of elemental carbon (EC) and organic carbon (OC), can result from a variety of incomplete combustion, such as cars, trucks, residential stoves, forest fires, etc. Some OC may be of biogenic sources or formed through gas-to-particle conversion in the atmosphere. Other minor constituents detected in fine PM include nitrate (NO_3^-), fly ash, and crustal material.

The Baltimore–Washington (B–W) corridor is one of the major metropolitan areas in the US Mid-Atlantic region. Utility plants and industries in the city of Baltimore, MD and Washington, DC, traffic on the highways, and residential cooking/heating can all contribute to fine aerosols in the corridor. The local (<100 km, roughly the B–W corridor) sources, however, may not fully explain the fine aerosol mass observed. For instance, it has been acknowledged that sources in the US Midwest can contribute to sulfate over the downwind Mid-Atlantic region (Ferman et al., 1981; Malm, 1992). One of the goals of the Maryland Aerosol Research and CHaracterization (MARCH-Atlantic) study is to attribute ambient $PM_{2.5}$ in the B–W corridor to possible sources. Our approaches include sampling 24-h chemically speciated $PM_{2.5}$ and aerosol precursor gases and interpreting the data considering chemistry and meteorology. A factor analysis model, UNMIX, is utilized to characterize major potential sources. The UNMIX-derived sources are studied further using an ensemble back trajectory (EBT) analysis to locate source regions. Special emphasis is put on partitioning local and regional contributions to the aerosol mass.

2. Sampling techniques

For a representative air quality in the B–W corridor, the sampling site was chosen at Fort Meade (FME) (39.10°N, 76.74°W; elevation 46 m MSL), a suburban site $\sim$30 km from both downtown Baltimore, MD and Washington, DC. There is no significant source within 1 km from the site. The field experiment took place over 2 years (June 1999–August 2001). One-hour average CO and SO_2 were measured continuously throughout the period using commercial instruments (Thermo Environment Instruments Model 48 and 43A) modified to improve sensitivity and selectivity (Chen et al., 2001). The detection limit for CO and SO_2 are $\sim$10 and $\sim$0.1 ppbv, respectively, and analytical uncertainties (AU) $<10\%$ are expected (95% confidence for a 60-min integration). Total reactive nitrogen (NO_y) primarily consists of NO_x ($NO+NO_2$) in an urban environment but also contains a variety of other oxidized nitrogen species such as HNO_3, NO_3^-, and peroxyacetyl nitrates (PANs). At FME, NO_y is measured with a commercial chemiluminescence detector (Thermo Environmental Instruments, Model 42), configured and operated by the Maryland Department of Environment under the USEPA guidance. A $\sim$3 m glass/Teflon tube used to sample ambient air and the stainless steel fittings remove HNO_3 and NO_3^- (Fehsenfeld et al., 1987). The quantity reported as 'NO_y' is then most probably the sum of NO, NO_2, and PAN.

$PM_{2.5}$ of 24-h average was sampled daily utilizing two sequential filter samplers (SFSs) in July, October, January, and April (except April 2001) chosen to represent summer, fall, winter, and spring, respectively. Twenty-four-hour average CO and SO_2 are also calculated to compare with the $PM_{2.5}$ data. The SFSs have been deployed in many field studies (e.g. Chow et al., 1996). The first SFS (SFS-1), equipped with a $PM_{2.5}$ size-selective inlet (Bendix/Sensidyne Model 240 cyclone) and an anodized-aluminum-coated HNO_3 denuder, uses a Teflon filter on one channel for determining dry $PM_{2.5}$ mass and concentrations of $\sim$30 elements (by X-ray fluorescence). The second channel of the SFS-1 contains a quartz filter followed by an NaCl-impregnated cellulose backup filter. The quartz filter is used to determine the concentration of water-soluble ions, while the cellulose filter is for capturing NO_3^- volatilized from the front quartz filter. Particulate nitrate (NO_3^-) reported is the sum of nitrate on front and backup filters. The second SFS (SFS-2) is designed to determine the $PM_{2.5}$ carbonaceous material, using two quartz filters (FQ and BQ) in series on one channel and a Teflon filter (FT) followed by a quartz backup filter (TBQ) on the second channel (Fig. 3). The thermal optical reflectance method (Chow et al., 1993) is applied to both front and backup quartz filters for determining EC and OC. EC detected on backup filters is usually below the detection limit but OC can be significant. OC on backup filters could result from two possibilities: (1) semi-volatile OC that evaporates off the front filter captured by the backup filter (Zhang and McMurray, 1987) and (2) gaseous volatile organic compounds (VOCs) absorbed by front and backup quartz filters (Turpin et al., 1994). The first possibility causes a negative bias while the second a positive bias if OC is determined solely using front quartz filters.

$HNO_{3(g)}$ is measured using a sequential gas sampler (SGS-1). Both channels of SGS-1 contain a quartz filter

followed by an NaCl-impregnated cellulose filter, and one of them contains a HNO_3 denuder upstream of the filters. Total nitrate (T-NO_3^-: $HNO_{3(g)}+NO_3^-$) is sampled by one channel but only NO_3^- by the other channel. The HNO_3 concentration can be determined from the difference between T-NO_3^- collected by the two channels. Another SGS (SGS-2) is used to measure $NH_{3(g)}$. In this case both channels contain a quartz filter followed by a citric-acid-impregnated cellulose filter, and one of them has a NH_3 denuder made up of critic-acid-coated parallel tubes upstream of the filters. The analytical uncertainty in a single measurement is typically within $\pm 10\%$ for a measured value which exceeds 10 times lower detection limits (Watson et al., 1995; Chow et al., 1996).

3. Field observations

As summarized in Table 1, the major mass contributing species include SO_4^{2-}, NO_3^-, NH_4^+, OC, and EC. Seasonal variation of SO_4^{2-} and SO_2 are shown in Fig. 1(a). The two highest monthly mean SO_4^{2-} concentrations appear in July 1999 and 2000; SO_2 in winter is twice as high as that in summer. Long-term monitoring at Washington, DC, within 30 km from FME, also indicates higher sulfate concentration in summer (Malm et al., 1994; IMPROVE, 2000). July 1999, which is extremely warm and dry compared to July 2000 and 2001, has the highest SO_4^{2-} concentration among the three summers. This could result from a stronger SO_2-to-SO_4^{2-} conversion due to the stronger insolation or a longer atmospheric lifetime of SO_4^{2-} due to the lack of precipitation. Fig. 2 shows the SO_2 diurnal profile in which a distinct mid-day maximum appears, especially in summer. Stehr et al. (2000) observed a similar pattern at Wye River, MD and suggested that SO_2 originates from distant sources; more intensive turbulence around noon mixes SO_2 downward from aloft, increasing the surface SO_2 concentration. The lifetime of SO_2 against oxidation can have a significant seasonal variation (Lusis et al., 1978). A shorter atmospheric lifetime in summer may explain the stronger diurnal contrast in SO_2 concentration. Long-range transport from the US Midwest is believed to be a major source of SO_2 and SO_4^{2-} in the Mid-Atlantic region. However, the correlation between SO_4^{2-} and SO_2 is weak in any season ($r^2<0.2$), and the variation of SO_4^{2-} only explains $\sim 20\%$ of the SO_2 variation. The high SO_2 concentration in winter can imply increased contributions from sources other than the US Midwest.

As shown in Fig. 1(b), HNO_3 and NO_3^- account, on average, for $<15\%$ of the measured NO_y. Therefore, uncertainty due to line losses of nitrate should be minor. Despite the uncertainty, two peaks and a mid-day low can be easily distinguished in the NO_y diurnal profile (Fig. 2). This diurnal profile is somewhat opposite to SO_2, suggesting different source regions for the two pollutants. The two peaks approximately agree with the morning and evening rush hours in time. NO_y concentration could be strongly influenced by on-road vehicle emissions. The correlation r^2 between 24-h average NO_y and CO, a good tracer for mobile emissions, is ~ 0.65. Considering the complex nature of NO_y and the AU, the significant positive correlation indicates proximate sources, likely traffic emissions. If so, the mid-day low

Table 1
Statistics of measurements at FME over eight sampling months between July 1999 and 2000. AU, FQ, BQ, and TBQ are defined in the text.

Species	Mean $\pm 1\sigma$ ($\mu g\,m^{-3}$)	# of samples	# of samples $>2\times$ AU
Mass	13.03 ± 7.74	266	266
SO_4^{2-}	4.59 ± 3.28	266	266
NO_3^-	1.04 ± 1.51	266	257
NH_4^+	1.75 ± 1.16	266	266
EC	1.06 ± 0.57	266	266
OC (FQ)	3.11 ± 1.41	266	265
OC (BQ)	0.72 ± 0.45	263	179
OC (TBQ)	1.43 ± 0.75	264	238
Cl	0.013 ± 0.072	266	16
Cl^-	0.035 ± 0.1	266	36
Na	0.072 ± 0.11	266	69
Na^+	0.04 ± 0.035	266	214
K	0.069 ± 0.13	266	266
K^+	0.056 ± 0.11	266	265
Mg	0.016 ± 0.018	266	28
Al	0.032 ± 0.037	266	219
Si	0.084 ± 0.098	266	227
P	0.0022 ± 0.0031	266	18
S	1.69 ± 1.22	266	266
Ca	0.026 ± 0.017	266	257
Ti	0.003 ± 0.0036	266	0
V	0.021 ± 0.024	266	0
Fe	0.064 ± 0.055	266	266
Mn	0.0017 ± 0.0016	266	63
Ni	0.0012 ± 0.0013	266	78
Cu	0.002 ± 0.0023	266	144
Zn	0.014 ± 0.013	266	265
As	0.0006 ± 0.0006	266	1
Se	0.002 ± 0.0017	266	148
Sr	0.0007 ± 0.0014	266	20
Br	0.0045 ± 0.0031	266	251
Ba	0.0083 ± 0.012	266	0
La	0.0085 ± 0.012	266	0
Pb	0.0047 ± 0.0034	266	118
$HNO_{3(g)}$	2.78 ± 1.94	231	209
$NH_{3(g)}$	0.58 ± 0.49	264	189
NO_y (ppb)	14.3 ± 6.3	194	—
CO (ppb)	314 ± 146	256	—
SO_2 (ppb)	3.8 ± 2.8	216	—

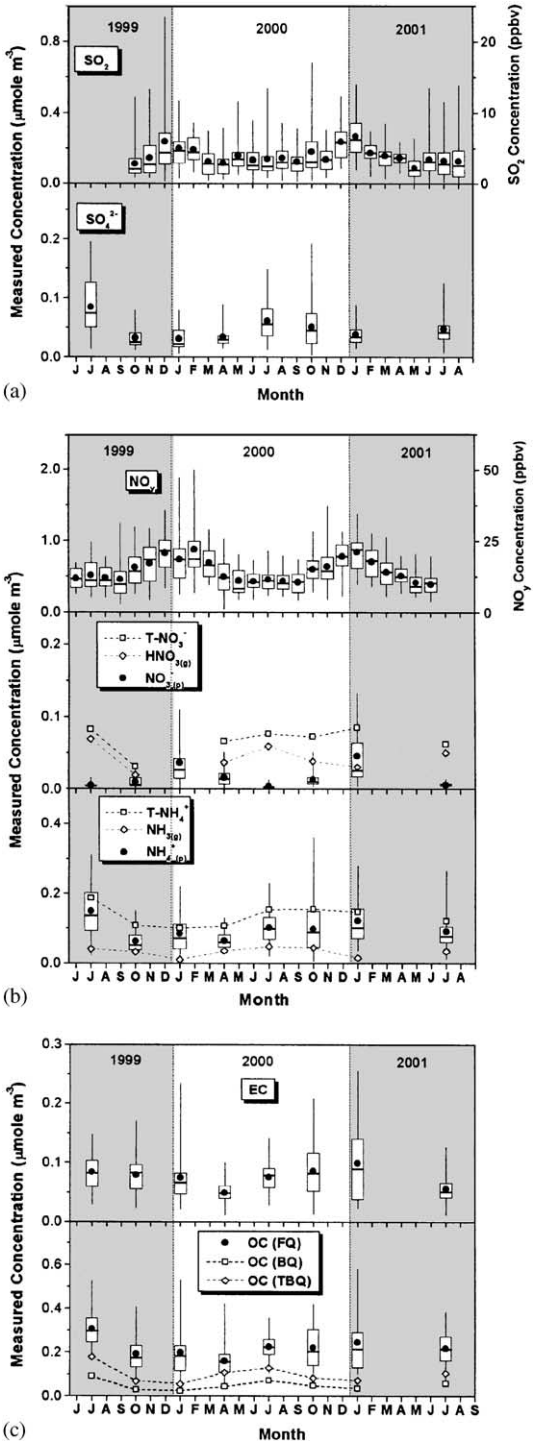

Fig. 1. Seasonal variation of 24-h average concentration of: (a) SO_2, SO_4^{2-}; (b) NO_y, NO_3^-, NH_4^+; and (c) EC, and OC at FME. Monthly means are indicated by circles and median values by short dashes. Boxes indicate the quartiles and vertical bars indicate the maximum and minimum. FQ, BQ, and TBQ are defined in the text.

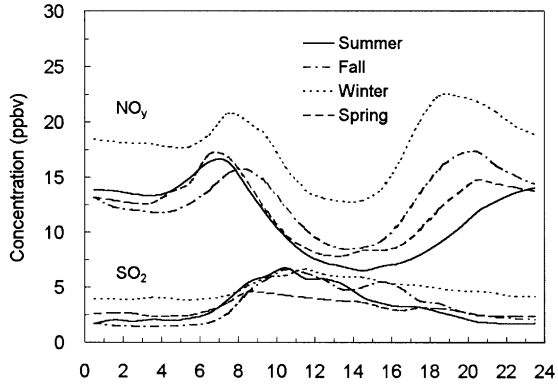

Fig. 2. Diurnal variation of SO_2 and NO_y at FME by season. Values are based on monthly means for each hour. Using monthly medians instead does not change the pattern significantly.

could reflect the stronger turbulent dilution into deeper PBL in the early afternoon. Nitrate is formed in the atmosphere predominantly through oxidation of NO_x. The summer–winter contrast of T-NO_3^- concentration is not significant though NO_y is $\sim$100% higher in winter than in summer (Fig. 1(b)). In summer, $>$90% of T-NO_3^- is HNO_3, but this fraction drops to $<$50% in winter. The gas/particle partitioning of T-NO_3^- depends on ambient temperature and relative humidity (Seinfeld and Pandis, 1998). At FME, temperature is lower in winter than in summer typically by 20–30°C; cooler weather favors the formation of particulate nitrate that becomes a significant fraction of $PM_{2.5}$ in winter. NH_3 concentration is particularly low in winter. NH_3 coexists with HNO_3 in summer, fall, and spring but seems to be depleted, forming particulate NH_4NO_3 as temperature decreases in winter (Fig. 1(b)).

Monthly mean EC and OC (FQ) concentrations do not show a clear seasonal cycle (Fig. 1(c)), but their 24-h values have much broader distributions in winter than in summer (Fig. 1(c)). In other words, EC and OC (FQ) levels in winter are driven by fewer but stronger events. The ratio of OC (BQ) or OC (TBQ) to OC (FQ) is lower in winter, and this could result from either a lower vapor pressure of semi-volatile OC or less VOC adsorption in winter. Chen et al. (2001) observed positive correlations ($r^2 \sim 0.50-0.84$) of EC with CO at FME and suggested that EC and CO have a co-located source. OC (FQ) is well correlated to EC only in winter with $r^2 \sim 0.8-0.9$. Mobile emission, known to contribute to OC, EC, and CO (Gertler et al., 2001), is believed to be a major source of carbonaceous particles at FME. The weak correlation between OC and EC in summer may suggest significant OC from non-combustion sources (e.g. biogenic and secondary OC) in summer.

4. Reconstructed and gravimetric $PM_{2.5}$ mass

Aerosol reconstructed mass is calculated to determine the extent of aerosol mass closure for the chemical species detected. A possible deviation between reconstructed mass and gravimetric mass results from OC since mass is sampled by Teflon filter but OC by quartz filter. On average, OC (BQ) and OC (TBQ) reaches $23\pm12\%$ and $49\pm19\%$ of OC (FQ), respectively. Quartz and Teflon filters behave differently relative to adsorbing VOC or evaporating semi-volatile OC, and this artifact cannot be ignored in estimating OC on Teflon filter. OC captured by a sequential quartz–quartz filter includes particulate OC (POC, low vapor pressure), semi-volatile OC (SVOC), and quartz-philic VOC (QVOC) (Turpin et al., 1994; Warner et al., 2001). Since Teflon generally absorbs much less VOC than quartz (Mader and Pankow, 2001), a Teflon–quartz filter likely obtains the same POC but less QVOC. Fig. 3 illustrates the plausible distribution of OC on the two sets of sequential filters. In case 1, QVOC$\gg$SVOC, OC on Teflon filter, OC (FT), can be estimated by subtracting OC (TBQ) from OC (FQ), assuming QVOC (FQ)$\sim$QVOC (TBQ). In case 2, SVOC$\gg$QVOC, Teflon–quartz and quartz–quartz filters would contain more equal OC, and thereby OC (FT) is better estimated by subtracting OC (TBQ) from OC (FQ)+OC (BQ). The difference between OC (FT) determined in cases 1 and 2 is exactly OC (BQ). The actual OC (FT) could be between the two extremes. Though there is no unarguable choice of OC, the OC (FT) defined in case 2 (the upper limit) is used hereafter with the understanding that $\sim$20% uncertainty may apply. The OC (FT) is multiplied by 1.4, average molecular weight per carbon weight (White and Roberts, 1977), to obtain the mass of organic matter (OM) before entering the $PM_{2.5}$ reconstructed mass. Nitrate that evaporates from single-layer Teflon filter could cause another deficit in $PM_{2.5}$ gravimetric mass. Volatile nitrate detected on backup filter (behind quartz) reaches the maximum in summer when nitrate is low at 1–2% of the $PM_{2.5}$ mass, and it becomes nearly zero in winter. Therefore the loss is expected to be minor.

Crustal material is another constituent of the $PM_{2.5}$. At FME, the five top aerosol elements primarily of crustal origin include, in decreasing order of overall $PM_{2.5}$ mass fraction, Si (0.64%), Fe (0.49%), Al (0.25%), Ca (0.2%), and Mg (0.12%). K (0.53%) contains 81% soluble K^+ that could originate from vegetative burning. Twenty-four-hour concentration of these elements remains much lower than the overall means except in a few events when the elemental concentration increases by 1–2 orders of magnitude (e.g., fireworks on 4 July lift K and K^+ levels). The mass of crustal material has to include oxygen associated with minerals and is estimated empirically (e.g. $1.89\times Al+2.14\times Si+1.4\times Ca+1.43\times Fe$) (Chow et al., 1996). Generally, crustal material contributes to $<3\%$ of the $PM_{2.5}$ mass. Na^+ is a good marker of marine aerosols. The mass fraction of Na^+ and Cl^- in $PM_{2.5}$ are 0.31% and 0.27%, respectively. Sea salt probably contributes to $<1\%$ of the $PM_{2.5}$ mass despite the proximity of FME to the US east coast.

Reconstructed mass calculated by summing sulfate, nitrate, ammonium, OM, EC and crustal material closely agrees with the gravimetric mass (Fig. 4: $r^2\sim0.94$, slope ~0.91). A deviation generally within 15% on low $PM_{2.5}$ days reflects analytical errors and the uncertainties in determining OC and nitrate. A more significant negative bias appears on high $PM_{2.5}$ days.

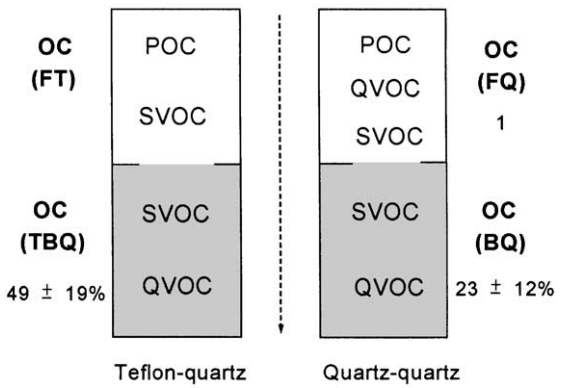

Fig. 3. Illustration of the idealized distribution of OC sampled by sequential Teflon–quartz and quartz–quartz filters. The arrow indicates the direction of sampling flow. All abbreviations are defined in the text. In this study, OC (BQ) and OC (TBQ) are $23\pm12\%$ and $49\pm19\%$ of OC (FQ), respectively.

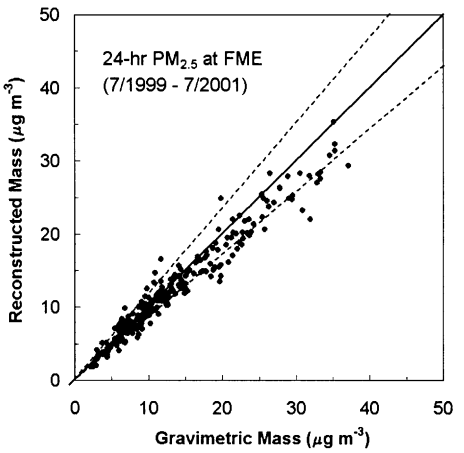

Fig. 4. Scatter plot of 24-h $PM_{2.5}$ gravimetric and reconstructed mass at FME. The solid and dashed lines indicate 1:1 and $\pm15\%$ lines, respectively.

Malm et al. (1994) and Rees et al. (2002) presented similar results and suggested that water could be part of the unidentified mass. The Teflon filters are weighed at 30–40% relative humidity but water associated with inorganic salts may not be removed completely. Turpin and Lim (2001) point out that OM/OC ratio in an urban environment can be higher than 1.4, and this provides another explanation for the 'missing' mass. Despite uncertainties, sulfate, nitrate, ammonium, and carbonaceous material combined explain a majority of the $PM_{2.5}$ gravimetric mass.

5. UNMIX factor analysis

Aerosol mass concentration measured at a receptor site is the sum of contribution from various sources. Ambient aerosol chemical composition usually bears information about the composition and relative contribution of each source. Chemical mass balance (CMB) techniques (e.g. Kowalczyk et al., 1982; Chow et al., 1992) assume a known number of sources and source compositions in a receptor region and uses a least-square approach to retrieve the source contributions from observations at the receptor site. Factor analysis methods (e.g. Koutrakis and Spengler, 1987; Chueinta et al., 2000; Song et al., 2001) do not utilize knowledge of sources but rely on a larger number of measurements. A factor analysis model, UNMIX, is utilized here in the attempt of apportioning $PM_{2.5}$ mass to possible sources. UNMIX depends on the 'edge' points (Henry, 1997). Using the data alone, UNMIX estimates the number of factors and the composition and contributions of these factors to the particulate loadings (Henry et al., 1999; Henry, 2000). One of the natural constraints imposed to the model is the non-negativity condition since both source compositions and contributions must be zero or positive. However, the effects of analytical errors require that UNMIX allows small negative values (Henry, 1997, 2000). UNMIX basically assumes linear combinations of all source contributions. Since complex atmospheric processes (e.g. deposition and gas-to-particle transformation) could weaken the source signatures, precautions have to be exercised in linking resolved factors to real source emissions. For example, Poirot et al. (2001) suggest that a coal-burning source could produce plumes of distinct compositions in summer and winter and split into two factors in the factor analysis.

Unlike remote sites, local (<100 km) and regional (100–1000 km) sources probably dominate the $PM_{2.5}$ mass at FME. The relatively short source–receptor distance is favorable for factor analysis since signals of source composition could gradually decay during atmospheric transport. Trace elements with concentration usually below the AU are not considered as UNMIX inputs. Only Na^+, K^+, K, Al, Si, S, Ca, Fe, Cu, Zn, Se, and Br have more than half of their values greater than twice the AU (Table 1). As suggested by their correlations in Table 2, Al, Si, and Ca are one group primarily of crustal origin while Se, Br, Zn, and Pb are another group likely linked to combustion sources. Almost no correlations are found between the two groups. Fe was assumed to be crustal material but its correlations with Cu, Pb, and Zn suggest other contributors. K and K^+ are also correlated to Br and Pb better than Si or Ca if three outlier points (4 July) are removed. To simplify the problem, we exclude Si, Al, Ca, and Na^+ from the model inputs since (1) crustal and marine sources are minor and contain little sulfate, nitrate and EC which result mostly from combustion and (2) crustal sources are diverse with their contributions likely dominated by special and rare events.

Using nine input variables, including gravimetric mass, SO_4^{2-}, NO_3^-, NH_4^+, OC (FT), EC, Se, Br, and Cu, a unique six-factor model is resolved by UNMIX, and their compositions and contributions are calculated. The model explains at least 91% of the variance of each of the fitting species. To test the model stability, an

Table 2
Correlation coefficients of species in $PM_{2.5}$ at FME. Numbers in bold indicate higher correlations ($r > 0.64$ or $r^2 > 0.41$)

(r)	Se	Br	Zn	Pb	K	K^+	Fe	Cu	Al	Si	Ca	Na^+
Se	1.00											
Br	**0.67**	1.00										
Zn	**0.64**	**0.79**	1.00									
Pb	0.58	**0.73**	**0.73**	1.00								
K	0.43	0.62	0.57	**0.75**	1.00							
K^+	0.47	**0.66**	0.61	**0.75**	**0.97**	1.00						
Fe	0.48	0.47	0.60	0.61	0.57	0.53	1.00					
Cu	0.22	0.28	0.34	0.44	0.31	0.32	**0.72**	1.00				
Al	0.10	0.04	0.01	0.17	0.38	0.24	0.47	0.11	1.00			
Si	0.09	0.02	0.04	0.11	0.30	0.16	0.46	0.05	**0.89**	1.00		
Ca	0.15	0.16	0.20	0.22	0.30	0.19	0.48	0.10	**0.65**	**0.66**	1.00	
Na^+	0.11	0.24	0.20	0.21	0.25	0.24	0.27	0.07	0.29	0.27	0.19	1.00

Table 3
Compositions of six factors contributing to $PM_{2.5}$ at FME

	F1	F2	F3	F4	F5	F6	Residue	r^2
Mass	**5.28**	0.93	**2.03**	**1.77**	**1.58**	0.19	—	0.98
NO_3^-	0.01 (0)	0.02 (2)	**0.99** (49)	0.02 (1)	0.05 (3)	−0.01 (−5)	—	0.99
SO_4^{2-}	**2.64** (50)	**0.70** (75)	0.10 (5)	0.16 (9)	0.47 (30)	0.11 (58)	—	0.99
NH_4^+	**0.83** (16)	**0.25** (26)	**0.33** (16)	0.08 (3)	0.13 (8)	0.00 (0)	—	0.99
EC	**0.19** (4)	**0.08** (9)	**0.17** (8)	**0.40** (23)	**0.09** (6)	0.05 (26)	—	0.94
OC (FT)	**0.57**	−0.04	**0.31**	**0.75**	**0.55**	0.04	—	0.91
$Cu \times 10^3$	0.07	0.14	0.2	0	−0.03	**1.92**	—	0.99
$Se \times 10^3$	0.3	**1.69**	0.21	0.07	−0.24	0.02	—	0.99
$Br \times 10^3$	**0.61**	**0.6**	**0.48**	**0.32**	**2.68**	0.06	—	0.99
OM	0.80 (15)	−0.06 (−6)	0.43 (21)	1.05 (59)	0.77 (49)	0.06 (32)	—	—
$Pb \times 10^3$	0.39	0.93	0.48	0.45	1.45	0.76	0.47	0.61
$Zn \times 10^3$	0.49	4.22	2.88	1.14	4.72	1.35	0.51	0.70
$Fe \times 10^3$	8.44	16.18	5.47	3.56	3.74	29.59	1.46	0.64
$K \times 10^3$	7.86	4.28	9	10.44	18.25	5.47	1.09	0.45
$K^+ \times 10^3$	6.65	3.78	11.07	8.98	13.45	4.51	−3.08	0.53
$Ni \times 10^3$	0.14	0.39	0.28	0.24	0.07	0.23	−0.11	0.40
$Mn \times 10^3$	0.17	0.67	0.4	0.15	0	0.3	0.1	0.50
$Al \times 10^3$	12.89	−0.58	−0.4	−1.77	−0.18	3.52	15.5	0.19
$Si \times 10^3$	28.56	1.76	−3.81	2.57	1.69	4.63	42.66	0.14
$Ca \times 10^3$	3.66	0.84	−0.32	2.6	1.89	0.94	15.83	0.10
$Na^+ \times 10^3$	1.97	−2.27	2.26	−4.33	10.43	0.41	33.27	0.09
CO	2.6	18.2	66.6	68.1	49.8	15.2	154.2	0.76
SO_2	−0.78	5.69	1.62	0.25	−2.19	−0.3	6.24	0.63

Values (in unit $\mu g\,m^{-3}$) shown are 2000 annual mean contributions of each factor. Values greater than twice the uncertainty calculated by UNMIX are noted in bold. Numbers in brackets indicate percentage of species relative to mass. The r^2 indicates correlation between measured and calculated concentrations.

arbitrary 1 month of data is removed from the UNMIX input, and this causes little difference in the output results. Table 3 shows the annual mean contribution of each factor (F1–F6) to mass and each species, from which one also obtains the factor composition. (Note that Table 3 shows the factor contributions averaged over the four sampling months in 2000, while Table 1 lists the overall mean concentrations of each species in the eight sampling months.) The monthly median as well as the 25th and 75th percentile contributions of each factor, relative to the 2000 annual mean, is shown in Fig. 5. UNMIX also estimates uncertainties in factor composition (Henry, 2000); values in bold in Table 3 are greater than twice the calculated uncertainty. The difference between the reconstructed mass ($SO_4^{2-} + NO_3^- + NH_4^+ + EC + OM$) and gravimetric mass in each factor is within $\pm 15\%$. A five-factor model using the same inputs is available but can explain only $\sim 80\%$ of the data variance. Adding K, Fe or Zn to build a six- or seven-factor model was unsuccessful, generating no solutions. K, Fe and Zn could partly originate from one or more sources that are unexpected in the model (e.g. crustal sources). We estimate the contributions of F1–F6 to species not included in the model by multiple linear regression (Table 3). The model explains the observations of Zn, Fe, and Pb ($r^2 > 0.6$) better than Al, Ca, and Si ($r^2 < 0.2$). Relatively large residues left from regressing Al, Ca, and Si suggest significant contributions from other sources. The model explains the CO variation ($r^2 = 0.76$) better than SO_2 ($r^2 \sim 0.6$ with negative loadings). The residue CO is $154.2\,\mu g\,m^{-3}$ (~ 130 ppbv), typical for BG CO level over Eastern North America (Poulida et al., 1991).

6. Source model discussion

Factors F1 and F2 together apportion $\sim 80\%$ of the sulfate. F2 differs from F1 by a higher Se/SO_4^{2-} ratio. Se is widely used as a tracer for coal burning and smelter operations (Rabano et al., 1989; Malm and Gebhart, 1997) that usually generate SO_2 and sulfate. SO_2 should dominate in a freshly emitted plume, but it is gradually converted to sulfate as the plume ages. The Se/SO_4^{2-} ratio is expected to be higher in fresh plumes than aged plumes. SO_2 is associated more closely with F2 than with any other factor (Table 3). Therefore, F1 and F2 suggest a thoroughly oxidized sulfate source and a partially oxidized sulfate source, respectively. The partially oxidized sulfate source should be geographically closer to FME to prevent a thorough oxidation before its plumes arrive at FME; this will be shown later

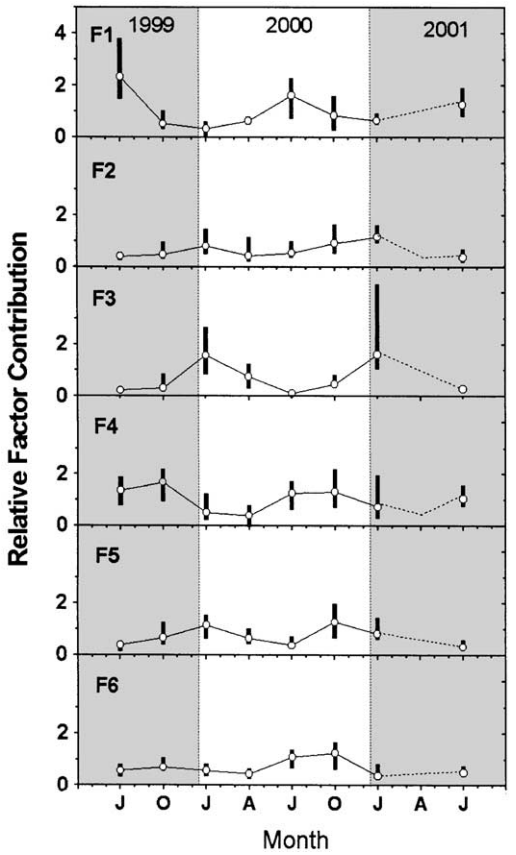

Fig. 5. Seasonal variation of contributions of six factors derived from UNMIX. Monthly medians are indicated by circles and quartiles by vertical bars. The dashed lines are added to reproduce the likely seasonal variation.

in the EBT analysis. F1 should be relatively far away, and its stronger contribution in summer is possibly due to more efficient long-range transport besides a higher SO_2-to-SO_4^{2-} conversion rate. It is noticed that F1 contains most unidentified mass. A large fraction of secondary sulfate is formed in aqueous phase (Pandis et al., 1992), and water associated with the sulfate may explain part of the 'missing' mass. The OC and EC apportioned to F1 probably have a proximate source region and share similar seasonal variations.

Factor F3 is the dominant source of secondary NH_4NO_3, and its contribution reaches a distinct maximum in winter. The suspected origin of NO_y, HNO_3, and NO_3^- is mobile emission. The EC/OC ratio in F3 is $\sim$0.55. Recent dynamometer and tunnel studies suggest EC/OC ratios of 0.75–3 for heavy-duty (diesel) vehicle emissions and lower values ($\sim$0.25–1) for light-duty (gasoline) vehicles (Gillies and Gertler, 2000; Gillies et al., 2001; Gertler et al., 2001). Since both types of vehicular traffic are closely located, our data based on 24-h sampling probably capture an average emission profile. Disregarding that EC/OC-separation can vary when different analytical methods are adopted (e.g. Chow et al., 2001), a 0.55 EC/OC ratio supports the association of F3 with a mobile source favoring gasoline vehicles. F4 features the same EC/OC ratio as F3 but shows a seasonal variation somewhat complementary to F3. Carbonaceous material is the single dominant species in F4. It is suggested that F4 represents the 'summer profile' of the mobile source, and it is separated from F3 (winter profile) because it contains no nitrate. The combination of F3 and F4 may better reproduce the real profile of the mobile source. This is confirmed as both the two factors apportion significant CO emission. A recent (1999) tunnel study carried out in the Mid-Atlantic region (Gertler et al., 2001) suggests an EC/CO ratio of 1.8×10^{-3} for light-duty vehicles and an unquantified high value ($>10^{-2}$) for diesels. The EC/CO ratio in F3 is close to 2.6×10^{-3}. In F4, a larger value of 5.9×10^{-3} may result from greater contributions from diesel emissions in summer. Ambient temperature is suggested to influence particulate emission of diesel engines through changing intake air density and air–fuel ratio (e.g. Chen et al., 2001). The F4 contribution reaches a maximum in fall rather than in summer. Factor contributions depend on both source strength and transport efficiency. Though the source strength of F4 should peak in summer, stronger summertime dispersion keeps its contribution low. The role of meteorology in the source-to-receptor transport will be discussed later.

Br and K are two important tracers in F5. Traditionally, Br is mostly attributed to mobile sources (Kowalczyk et al., 1982; Chow et al., 1992). Cadle et al. (1999), however, suggest that vehicles manufactured after 1990 have substantially reduced the Br and Pb emissions. Tunnel studies (Gillies et al., 2001; Gertler et al., 2001) suggest that diesel vehicles dominate Br emission with a Br/EC ratio $\sim10^{-4}$. The Br/EC ratio in F5 is higher than that by 2–3 orders of magnitude. Malm and Gebhart (1997) note a strong correlation of Br with atmospheric absorption at rural sites of low transportation and suggest that the Br is related to residential wood burning. Turn et al. (1997) report an EC/OC ratio ranging from 0.1 to 0.3 and a mean Br/EC (also Pb/EC) ratio $\sim10^{-3}$ for various types of wood burning. These values are close to what we find in F5. The F5 peak in winter and contribution to K and K^+ further support its association with vegetative burning. F5 is expected to contain CO but not high sulfate. However, a positive correlation between sulfate and Br is observed here and in Malm and Gebhart (1997). Sources of sulfate and wood smoke may have some overlap spatially.

F6 is relatively minor, contributing $\sim$2% of the $PM_{2.5}$ mass. This factor suggests another sulfate source rich in

Cu and Fe. Given that the US Northeast is a highly industrialized region, F6 could be caused by industrial emissions, such as iron/copper smelters. Compared to F2, F6 contribution is higher in fall and summer when long-range transport is generally more efficient.

Justifying the choice of the number of factors is difficult in factor analysis. Using too few factors may combine sources of different nature together while using too many factors make a real factor dissociate into two or more non-physical sources. Kowalczyk et al. (1982) employed a CMB model of seven sources, including soil, limestone, motor vehicle, coal, oil, refuse, and marine sources, to explain 'primary' total suspended particle (TSP) mass in Washington, DC. Each of the last three sources contributes to only ~1% of the TSP. Soil is quite dominant but appears mostly in coarse particles. For fine particles, it is essentially a six-source approach if one excludes soil, limestone, and marine sources but adds secondary sulfate and nitrate. Though the sources selected are not identical to the UNMIX solution here, six factors seem to be sufficient for including major $PM_{2.5}$ contributors (except sea salt and crustal) in the B–W corridor (e.g. Song et al., 2001). The factors found here have such distinct characteristics that six factors are thought to be necessary as well.

7. EBT analysis

Analyzing meteorology associated with episodes of high or low factor contribution can provide insights into source locations. For example, the wind rose analysis is used to identify directions from which pollutants arrive at a receptor site (Chow et al., 1996; Chueinta et al., 2000). However, on the meteorological microscale surface wind can be misleading since natural terrain, vegetation and man-made structures can influence surface flow significantly. Mean streamlines of synoptic and meso-scale circulation, important for long-range transport, are usually better described by air parcel trajectories. A back trajectory traces an air parcel backward in time from a receptor; source contributions usually depend on the air parcel's residence time over the source regions (Moy et al., 1994; Poirot et al., 2001; Polissar et al., 2001).

The Hybrid Single-Particle Lagrangian Integrated Trajectories (HY-SPLIT) model (Draxler, 1991) was used in this study to generate air parcel back trajectories. The model input includes observational (actual) wind field data, Eta Data Assimilation System (EDAS, model range: 20–55°N, 60–130°W, 0–~6 km; see http://www.arl.noaa.gov/ready/hysplit4.html). Comparing HY-SPLIT calculated back trajectory with the path of actual tracer plumes suggests a potential error of 20–30% of total travel distance (Draxler, 1991). An EBT approach is developed to cooperate with the 24-h $PM_{2.5}$ data. In this approach, the eastern US (30–55°N, 65–105°W) is gridded into $1 \times 1^{\circ}$ areas (~40 km × 40 km). The vertical dimension from surface to 4 km is divided into eight 500 m layers, and therefore 8000 cells are used in total. Considering that transport over a regional scale (~1000 km) generally takes 2–3 days and the lifetime of fine particles against wet deposition is ~1 week, 72-h back trajectories (endpoints separated by ~6 min) are calculated in this study. Trajectories were calculated every 2 h to capture diurnal-scale meteorology. To better consider dispersion and mixing across PBL, the initial height of back trajectories is chosen at 500 m above FME (~950 mbar). The history of incoming air on a particular day (i.e. the daily average back trajectory) is determined by counting endpoints of the 12 back trajectories in that day to calculate 'probability field'. A probability field is a matrix of ratios of air parcel residence time in each cell over ensemble time:

$$\text{Ensemble time} = 72\,\frac{\text{hour}}{\text{trajectory}} \times 12\,\frac{\text{trajectory}}{\text{day}} \times N \text{ sampling days}$$

Using this concept we can calculate daily ($N = 1$), monthly ($N = 30$), or annual probability fields for the receptor site. This 'averaging' approach reduces random errors created in each trajectory calculation. Two kinds of probability fields, 'background' (BG) and 'high-day' (HD), are especially useful in this study. The BG probability field is an overall average, containing trajectories of all 266 sampling days. In constructing a HD probability field, only days of a relatively strong factor or source contribution are selected. The difference between HD and BG probability field, referred to as 'incremental' probability field, contains information about the source location.

The chance of contributing distinguishably is different for each factor. The criterion for selecting HD is a compromise; including too many days will weaken the signal of a factor while including too few days may produce unrepresentative results. The similarity between HD and BG probability fields can be estimated from $\|\text{HD–BG}\|$, sum of the absolute values of the incremental matrix elements. (Notice that the sum of incremental matrix elements always vanishes.) Starting with a HD using any daily probability field, $\|\text{HD–BG}\|$ is usually ~2; it is gradually reduced to zero as the HD includes more and more days until finally HD becomes BG. We calculate a series of HD probability fields for F1–F6, starting from the day of the strongest factor contribution, then adding the second, and so on. Fig. 6 shows the $\|\text{HD–BG}\|$ of F1–F6 as a function of number of HD included, in comparison with that obtained by adding days selected randomly (RD). The curves representing factors are above the 'random' curve, and this indicates that daily ensemble back trajectories do contain certain degrees of source signal. The F1 curve

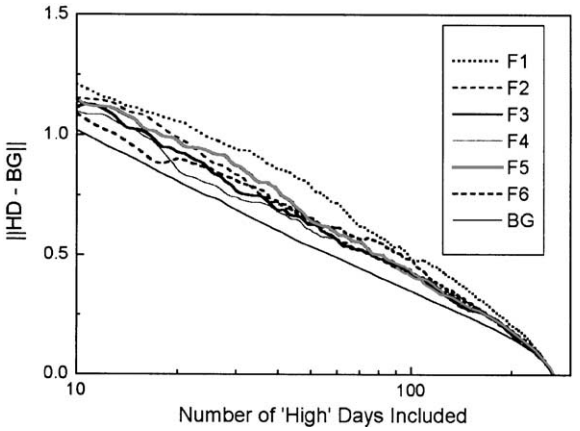

Fig. 6. Deviation of HD from RD probability field as a function of number of days included in HD. F1-F6 indicate the six factors derived by UNMIX. RD indicates the 'random' curve.

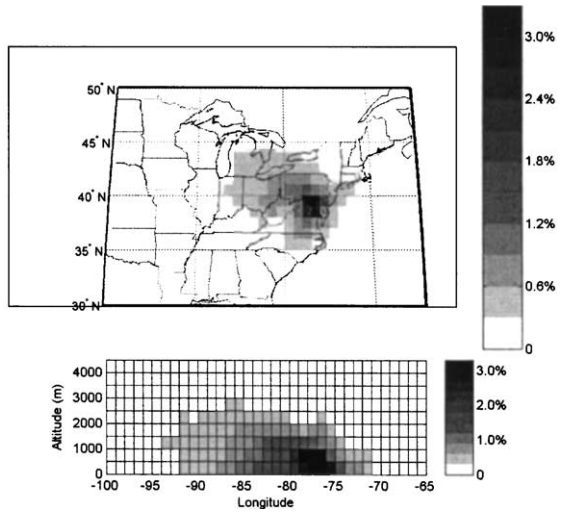

Fig. 7. The BG probability field for FME using back trajectories of 266 sampling days between July 1999 and 2001.

shows the weakest slope, suggesting that the back trajectory leading to a strong contribution of F1 is most favored. In this study, we adopt the HD probability field in which $\|HD–BG\|$ equals 0.75 since (1) $\|HD–BG\|$ between 0.5 and 1 is where the factor curves differ from the random curve most, (2) $\|HD–BG\|/\|BG\|$ ratio of 0.75 means a HD $\sim$75% different from BG, which provides an adequate contrast between the HD and BG field, and (3) making $\|HD–BG\|$ constant for all six factors facilitate analyzing the extent of source region from the incremental probability field. Therefore, the number of days (and the fraction out of 266 days) used to construct HD for F1–F6 is 56 (21%), 37 (14%), 34 (13%), 29 (11%), 42 (16%), and 38 (14%), respectively. Due to inherent uncertainties, the calculated incremental probability field may not indicate the exact contribution of each area within the modeled domain. It is, however, useful for comparing direction of transport and extent of source region of the six factors.

Since the size of each cell in the EBT analysis is different and depends on its latitude, it is not the probability but the probability density (probability divided by the cell's size) that better represents the history of air parcels. To compensate for this, the probability reported hereafter has been divided by the cosine of its latitude. (This causes limited differences in the mid-latitude region, and hereafter we use the term probability with the understanding that it is relative probability density.) Fig. 7 shows the BG probability field. The original three-dimensional matrix is squeezed into two two-dimensional charts in order to present its horizontal and vertical components separately. The highest probability of 5–6% is at FME where all back trajectories initiate, and higher value extends to its northwest. Throughout the sampling period, northwesterly transport is so dominant that emissions from upwind west Pennsylvania, Ohio, and Michigan may have the greatest impact on our sampling site. In the vertical dimension, the trajectory ensemble generally spends equal time between 0 and 1.5 km (AGL). Usually, an air parcel entrains more pollutants if it stays longer near the surface in source regions. However, a high probability of back trajectory at the lowest level (0–499 m) around the receptor site, especially in summer, could indicate low-level convection that dilutes pollutants released locally.

The incremental probability fields of F1–F6 are shown in Figs. 8(a)–(f), respectively (only positive values shown). In Fig. 8(a), high probabilities appear in a broad area west of FME but excluding FME. Longer residence time of air parcels over FME is coupled with lower factor contribution. This confirms that F1 is nonlocal. Regions of higher probability include the Ohio River Valley and Pittsburgh area; trajectories stay near the surface when passing through these suspected source regions. F1 represents regional sulfate that likely originates from the Midwest and moves into the Mid-Atlantic region along the northern border of Maryland. Significant OC and EC in F1 explain most of the nonlocal carbonaceous aerosols that could originate from the Midwest. In contrast, the incremental probability field of F2, another sulfate contributor, indicates a strong local maximum (Fig. 8(b)). F2 generally contributes more strongly under stagnant or stable conditions when winds are weak and trajectories move slowly in the PBL. This supports the assumption that F2 represents a nearby sulfate source. The incremental probability is higher at north of FME, and this fine feature links F2 to the cities of Baltimore and Philadelphia, both of which have several coal-burning

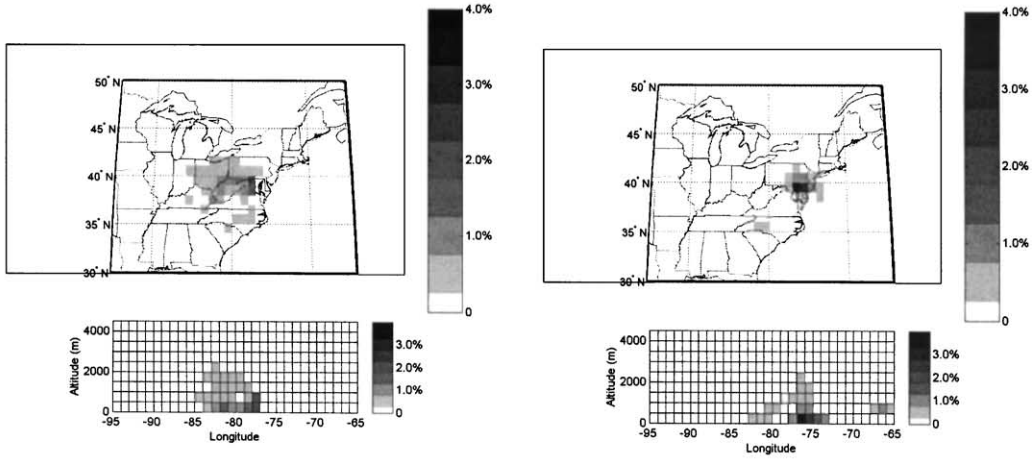

(a) F1 (regional sulfate)

(b) F2 (Se, sulfate)

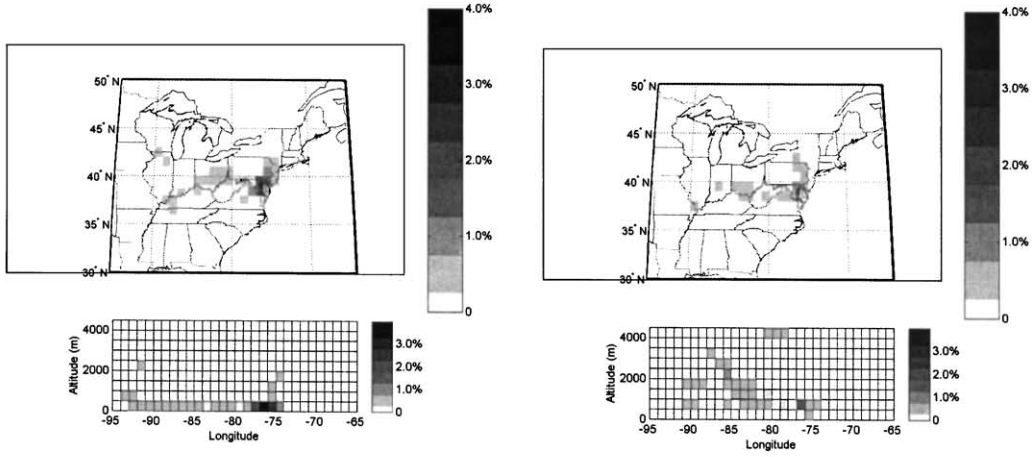

(c) F3 (secondary nitrate, mobile)

(d) F4 (mobile)

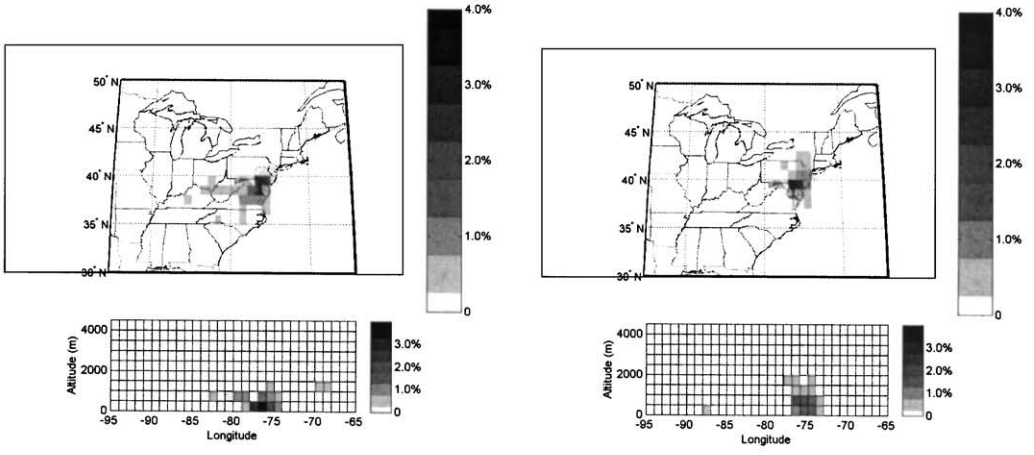

(e) F5 (Br, K, wood smoke)

(f) F6 (Cu, Fe, and sulfate)

Fig. 8. (a)–(f) The incremental probability fields (HD–BG) calculated for six $PM_{2.5}$ contributing factors at FME.

power plants. The F2 contribution is weaker in summer when turbulence in the PBL is strong. An incremental probability field using only summer trajectories suggests that stronger F2 contribution in summer is usually related to atmospheric subsidence associated with synoptic scale high-pressure systems.

F5 represents a proximate source as well (Fig. 8(e)). Compared to F2, the incremental probability of F5 is less concentrated around FME, and therefore F5 may have a broader source region. Higher probability remains at low levels, extending from Washington, DC to rural areas in central and western Virginia, where residential wood stoves and fireplaces are often utilized in winter. According to the National Emission Trend 1996 (USEPA, 2000), the fraction of CO emission from residential wood burning is higher in Virginia (13%) and West Virginia (10%) than in Maryland (3%), Pennsylvania (4%), Delaware (2%) and New Jersey (1%). F5 contributes more strongly in winter probably due to the stronger emissions and more stable PBL. The origin of F6 seems to come from northeast of FME (Fig. 8(f)). Between New York and Philadelphia is a heavily industrialized corridor. Factories such as blast furnaces and iron smelters can release trace metals (Cu and Fe) appearing in F6. A dispersion model with finer spatial resolution is required to investigate contributions of these point sources.

In Fig. 6, the incremental probability fields of F3 and F4 contain the lowest degree of source signature (e.g. their curves are closest to the 'random' curve). These two factors' contributions depend least on the air parcel back trajectory, implying that the mobile emissions are too close to FME to be resolved by the EBT analysis. (Note that major highways within a few miles from FME include I-95, MD-295, US-1 (west), MD-175 (northeast), and MD-32 (south)). F3, similar to F2, has a local maximum probability at the ground level but shows little preferred direction of transport (Fig. 8(c)). The F4 probability field shows no specific region of dominance (Fig. 8(d)). F3 and F4 are thought to represent the same mobile source, but they dominate in different seasons. F3 is stronger in winter when the high contribution of a local source is generally caused by stable near-surface conditions. F4 contributes more in summer and fall when air parcels spend less time within the PBL, and atmospheric subsidence under the influence of high-pressure systems is often responsible for strong local contributions. The EBT analysis shown in Figs. 8(c) and (d) clearly corroborates these concepts.

8. Conclusions

Twenty-four-hour average, chemically speciated $PM_{2.5}$ data acquired at Fort Meade, Maryland, over a 2-year period, including eight seasonally representative months, are presented and analyzed here. Sulfate, nitrate, ammonium, and carbonaceous material combined explain $>90\%$ of the $PM_{2.5}$ mass. Ammonium sulfate dominates in summer ($>50\%$) but its mass fraction decreases to $\sim 30\%$ in winter when more ammonium nitrate is formed due to lower ambient temperature. Carbonaceous material accounts for 30–45% of the $PM_{2.5}$ mass. Good correlations between EC, CO, and NO_y are observed; EC and a large fraction of OC likely result from mobile emissions. Crustal material and sea salt aerosols are minor, contributing $<5\%$ of the $PM_{2.5}$ mass. Reconstructed aerosol mass closely agrees with the gravimetric mass despite a deficit partly due to unaccounted species such as water.

A model of six factors that contribute to the $PM_{2.5}$ mass is constructed along with source compositions and associated contributions by a factor analysis technique, UNMIX, using mass, SO_4^{2-}, NO_3^-, NH_4^+, EC, OC, Br, Se, and Cu as the model inputs. Two factors appear to represent contribution of an aged sulfate source and a fresh SO_2/sulfate source. The model also suggests contributions from wood burning and Cu/Fe processing plants. Mobile emission is represented by two factors distinguished by their nitrate content, and this implies that a source with its composition varying temporally may dissociate into two or more factors in the factor analysis. We study source locations for the six factors identified using an EBT analysis that calculates the difference between probability fields of air parcel back trajectories on BG and HD. The aged sulfate source is more regional in character, resulting from emissions in the Midwest, while the fresh SO_2/sulfate mixture likely originates from proximate urban areas north of FME. Wintertime wood burning occurs more in rural areas of Virginia and West Virginia, and the mobile-related factors are dominated by traffic emissions on the nearby highways. Fig. 9 shows the $PM_{2.5}$ mass contributions, by

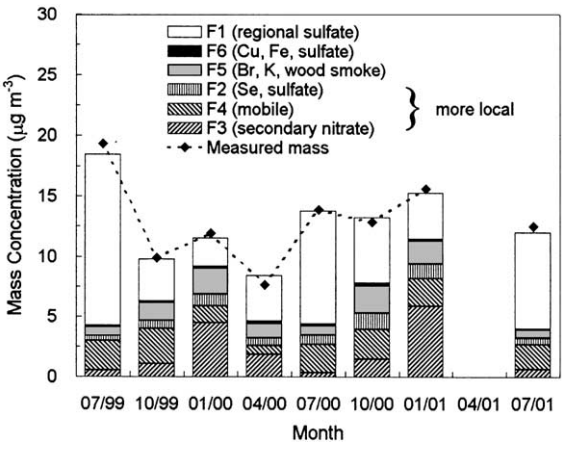

Fig. 9. Monthly contribution of six factors calculated by UNMIX to the $PM_{2.5}$ mass at FME.

season, from the six factors calculated by the UNMIX. Summertime fine PM is dominated by the regional sulfate source, and the fraction of local contribution, mobile sources plus local sulfate, increases from $<30\%$ in summer to $>60\%$ in winter. Though high $PM_{2.5}$ episodes were observed in both summer and winter, the relative importance of local and regional sources could be very different. This finding may affect the strategies for controlling fine PM and haze pollution in the Mid-Atlantic region.

Acknowledgements

This work was supported in part by Baltimore Gas and Electric Company and Potomac Electric Power Company through Electric Power Research Institute and Maryland Industrial Partnerships. Additional analyses were supported by USEPA Grant Number R826373. The authors thank Maryland Department of Environment for additional support at sampling site. P. Mueller is the project manager. T. Aburn, W. Butler, E. Gluth, S. Kohl, F. Pluciennik, D. Preece and J. Quinn provided substantive contributions. The authors also appreciate inspiring discussions with R. Poirot at Vermont Department of Environmental Conservation.

References

Cadle, S.H., et al., 1999. Composition of light-duty motor vehicle exhaust particulate matter in the Denver, Colorado area. Environmental Science and Technology 33, 2328–2339.

Chen, L.-W.A., Doddridge, B.G., Dickerson, R.R, Muller, P.K., Chow, J.C., Butler, W.A., 2001. Seasonal variations in elemental carbon aerosol, carbon monoxide, and sulfur dioxide: implications for sources. Geophysical Research Letters 28 (9), 1711–1714.

Chow, J.C., Waston, J.G., Lowenthal, D.H., Solomon, P.A., Magliano, K.L., Ziman, S.D, Richards, L.W., 1992. PM_{10} source apportionment in California's San Joaquin Valley. Atmospheric Environment 26A, 3335–3354.

Chow, J.C., Waston, J.G., Pritchett, L.C., Pierson, W.R., Frazier, C.A., Purcell, R.G., 1993. The DRI thermal/optical reflectance carbon analysis system: description, evaluation and applications in US air quality studies. Atmospheric Environment 27, 1185–1201.

Chow, J.C., Watson, J.G., Lu, Z., Lowenthal, D.H., Frazier, C.A., Solomon, P.A., Thuillier, R.H., Magliano, K., 1996. Descriptive analysis of $PM_{2.5}$ and PM_{10} at regionally representative locations during SJVAQS/AUSPEX. Atmospheric Environment 30, 2079–5102111.

Chow, J.C., Watson, J.G., Crow, D., Lowenthal, D.H., Merrifield, T., 2001. Comparison of IMPROVE and NIOSH carbon measurements. Aerosol Science and Technology 34 (1), 1–12.

Chueinta, W., Hopke, P.K., Paatero, P., 2000. Investigation of sources of atmospheric aerosol at urban and suburban residential areas in Thailand by positive matrix factorization. Atmospheric Environment 34 (20), 3319–3329.

Dockery, D.W., Pope, C.A., Xu, X.P., Spengler, J.D., Ware, J.H., Fay, M.E., Ferris, B.G., Speizer, F.G., 1993. An association between air-pollution and mortality in 6 United States cities. New England Journal of Medicine 329, 1753–1759.

Draxler, R.R., 1991. The accuracy of trajectories during ANATEX calculated using dynamic model analysis versus rawinsonde observations. Journal of Applied Meteorology 30, 1466–1467.

Fehsenfeld, F.C., Dickerson, R.R., Hubler, G., Luke, W.T., Nunnermacker, L.J., Williams, E.J., Roberts, J.M., Calvert, J.G., Curran, C.M., Delany, A.C., 1987. A ground-based intercomparison of NO, NO_x, and NO_y measurement techniques. Journal of Geophysical Research 92, 14710–14722.

Ferman, M.A., Wolff, G.T., Kelly, N.A., 1981. The nature and sources of haze in the Shenandoah Valley/Blue Ridge Mountains area. Journal of Air Pollution Control Association 31 (10), 1074–1082.

Gertler, A.W., et al., 2001. Sampling of ambient diesel particulate matter in the Tuscarora Mountain Tunnel, Pennsylvania. Final report prepared for Health Effects Institute, Cambridge, MA, Desert Research Institute, Reno, NV.

Gillies, J.A., Gertler, A.W., 2000. Comparison and evaluation of chemically speciated mobile source $PM_{2.5}$ particulate matter profiles. Journal of the Air and Waste Management Association 50, 1459–1480.

Gillies, J.A., Gertler, A.W., Sagebiel, J.C., Dippel, W.A., 2001. On-road $PM_{2.5}$ and PM_{10} emissions in the Sepulveda Tunnel, Los Angeles, California. Environmental Science and Technology 35, 1054–1063.

Henry, R.C., 1997. History and fundamentals of multivariate air quality receptor models. Chemometrics and Intelligent Laboratory Systems 37, 37–42.

Henry, R.C., 2000. UNMIX theory and applications. In: Willis, R.D. (Ed.), Final Report of Workshop on UNMIX and PMF as Applied to $PM_{2.5}$. United States Environment Protection Agency, Washington, EPA/600/A-00/48.

Henry, R.C., Park, E.S., Spiegelman, C.H., 1999. Comapring a new algorithm with the classical methods for estimating the number of factors. Chemometrics and Intelligent Laboratory Systems 48, 91–97.

Interagency Monitoring of Protected Visual Environments (IMPROVE), 2000. Spatial and seasonal patterns and temporal variability of haze and its constituents in the Unites States: Report III, ISSN: 0737-5352-47.

Koutrakis, P., Spengler, J.D., 1987. Source apportionment of ambient particles in Steubenville, OH using specific rotation factor analysis. Atmospheric Environment 21, 1511–1519.

Kowalczyk, G.S., Gordon, G.E., Rheingrover, S.W., 1982. Identification of atmospheric particulate sources in Washington, D.C. using chemical element balances. Environmental Science and Technology 16, 79–90.

Lusis, M.A., Anlauf, K.G., Barrie, L.A., Wiebe, H.A., 1978. Plume chemistry studies at a Northern Alberta Power Plant. Atmospheric Environment 12, 2429–2437.

Mader, B.T., Pankow, J.F., 2001. Gas/solid partitioning of semivolatile organic compounds (SOCs) to air filters. 3. An analysis of gas adsorption artifacts in measurements of atmospheric SOCs and organic carbon when using Teflon membrane filters and quartz fiber filters. Environmental Science and Technology 35, 3422–3432.

Malm, W.C., 1992. Characteristics and origins of haze in the continental United States. Earth-Science Review 33, 1–36.

Malm, W.C., Gebhart, K.A., 1997. Source apportionment of sulfur and light extinction using receptor modeling techniques. Journal of the Air and Waste Management Association 47, 250–268.

Malm, W.C., Sisler, J.F., Huffman, D., Eldred, R.A., Cahill, R.A., 1994. Spatial and seasonal trends in particle concentration and optical extinction in the United States. Journal of Geophysical Research 99 (D1), 1347–1370.

Moy, L.A., Dickerson, R.R., Ryan, W.F., 1994. How meteorological conditions affect tropospheric trace gas concentrations in rural Virginia. Atmospheric Environment 28, 2789–2800.

Pandis, S.N., Seinfeld, J.H., Pilinis, C., 1992. Heterogeneous sulfate production in an urban fog. Atmospheric Environment 26A, 2509–2522.

Poirot, R.L., Wishinski, P.R., Hopke, P.K., Polissar, A.V., 2001. Comparative application of multiple receptor methods to identify aerosol sources in northern Vermont. Environmental Science and Technology 35, 4622–4636.

Polissar, A.V., Hopke, P.K., Poirot, R., 2001. Atmospheric aerosol over Vermont: chemical composition and sources. Environmental Science and Technology 35, 4604–4621.

Poulida, O., Dickerson, R.R., Doddridge, B.G., Holland, J.Z., Wardell, R.G., Watkins, J.G., 1991. Trace gas concentrations and meteorology in rural Virginia: 1. Ozone and carbon monoxide. Journal of Geophysical Research 96 (D12), 22461–22475.

Rabano, E.S., Castillo, N.T., Torre, K.J., Solomon, P.A., 1989. Speciation of arsenic in ambient aerosols collected in Los Angeles. Journal of the Air and Waste Management Association 39, 76–80.

Rees, S.L., Takahama, S., Robinson, A.L., Khlystov, A., Pandis, S.N., 2002. Seasonal composition of $PM_{2.5}$ and performance of the Federal Reference Method in Pittsburgh. In: $PM_{2.5}$ and Electric Power Generation: Recent Findings and Implications. Summaries of a Conference Sponsored by National Energy Technology Laboratory, Pittsburgh, PA, 9–10 April, pp. 69–70 (see http://www.netl.doe.gov/publications/proceedings/02/pm25/).

Seinfeld, J.H., Pandis, S.N., 1998. Atmospheric Chemistry and Physics. Wiley, New York, pp. 533.

Song, X.-H., Polissar, A.V., Hopke, P.K., 2001. Sources of fine particle composition in the northeastern US. Atmospheric Environment 35, 5277–5286.

Stehr, J.W., Dickerson, R.R., Hallock-Waters, K.A., Doddridge, B.G., Kirk, D., 2000. Observation of NO_y, CO, and SO_2 and the origin of reactive nitrogen in the eastern United States. Journal of Geophysical Research 105 (D3), 3553–3563.

Turn, S.Q., Jenkins, B.M., Chow, J.C., Pritchett, L.C., Campbell, D., Cahill, T., Whalen, S.A., 1997. Elemental characterization of particulate matter emitted from biomass burning: wind tunnel derived source profiles for herbaceous and wood fuels. Journal of Geophysical Research 102 (D3), 3683–3699.

Turpin, B.J., Lim, H.-J., 2001. Species contributions to $PM_{2.5}$ mass concentrations: revising common assumptions for estimating organic mass. Aerosol Science and Technology 35, 602–610.

Turpin, B.J., Huntzicker, J.J., Hering, S.V., 1994. Investigation of organic aerosol sampling articles in the Los Angeles basin. Atmospheric Environment 28, 3061–3071.

United States Environmental Protection Agency, 2000. National air pollutant emission trends: 1990–1998. EPA-454/R-00-002 (see http://www.epa.gov/ttn/rto/areas/net.htm).

Warner, K.S., Eatough, D.J., Stockburger, L., 2001. Determination of fine particulate semi-volatile organic material at three eastern US sampling sites. Journal of the Air and Waste Management Association 51, 1302–1308.

Watson, J.G., Lioy, P.J., Mueller, P.K., 1995. The measurement process: precision, accuracy, and validity. In: Cohen, B., Hering, S.V. (Eds.), Air Sampling Instruments for Evaluation of Atmospheric Contaminants, 8th Edition. American Conference of Governmental Industrial Hygienists, Cincinnati, OH.

White, W.H., Roberts, P.T., 1977. On the nature and origins of visibility-reducing aerosols in the Los Angeles air basin. Atmospheric Environment 11, 803–812.

Zhang, X.Q., McMurray, P.H., 1987. Theoretical analysis if evaporative losses from impactor and filter deposites. Atmospheric Environment 21, 1779–1789.